Nanoscale

PAPER

View Article Online
View Journal | View Issue

Cite this: *Nanoscale*, 2025, **17**, 21546

Computational design of metal–organic frameworks with triangular adsorbaphores for highly selective adsorption of *m*-xylene

Saad Aldin Mohamed and Jianwen Jiang *

Received 31st May 2025,
Accepted 14th August 2025

DOI: 10.1039/d5nr02310f

rsc.li/nanoscale

Separation of xylene isomers, serving as indispensable feedstock in the petrochemical industry, is important but significantly challenging due to their similar physicochemical properties. With readily tunable network structures and chemical functionalities, metal–organic frameworks (MOFs) are promising for separation and many other potential applications. Here, we computationally design 150 lanthanide-based MOFs with one-dimensional triangular nanopores by varying metal compositions. Compared with *p*-xylene (*p*X) and *o*-xylene (*o*X), *m*-xylene (*m*X) exhibits the strongest interaction with these MOFs, as it can wedge at the vertices of triangular nanopores. Because of such shape-matching, highly selective adsorption of *m*X is observed, with exceptional *m*X/*o*X and *m*X/*p*X selectivities. Remarkably, the nanopore size of these MOFs can be systematically adjusted through different metal combinations, achieving efficient xylene separation. The proposed design strategy would facilitate the development of new MOFs and other framework materials for highly selective xylene separation.

Introduction

Among three xylene isomers, *p*-xylene (*p*X) has the highest market value compared to *m*-xylene (*m*X) and *o*-xylene (*o*X). *p*X is used to produce terephthalic acid (PTA), which is a key precursor for manufacturing polyethylene terephthalate (PET) resin. Nevertheless, there is a growing industrial demand for *m*X as a raw material to produce isophthalic acid (PIA).[1] PIA is a modifier in the production of PET, in addition to being used in the manufacturing of many other commodities. Therefore, it is of central importance to separate xylene isomers in the petrochemical industry. Because of the similar physicochemical properties of the isomers, xylene separation by thermally driven distillation is extremely energy intensive. In this context, adsorption turns out to be an efficient technology for xylene separation. A notable example is an industrial unit operation called "MX Sorbex", which was invented by Honeywell UOP specifically to produce high purity *m*X, occupying over 90% share of the *m*X production market.[2] In industrial xylene separation, zeolite adsorbents are utilized but they offer only modest separation performance.[3] There has been a continual quest to develop alternative adsorbents that provide high performance and operational flexibility for xylene separation.

With remarkable tunability in pore size and shape, structural topology, as well as chemical functionality, metal–organic frameworks (MOFs) are intriguing adsorbents for separation and many other potential applications.[4,5] Several experimental[6–10] and computational[11–14] studies have demonstrated the utilization of MOFs for xylene separation, primarily targeting the selective adsorption of *p*X. However, fewer efforts have been devoted to the separation of *m*X. The objective of this work is to design MOFs for highly selective adsorption of *m*X from xylene isomers. We focus on a unique branch of MOFs comprising rare-earth (RE) metals, in which the metal node may consist of a single- or multinuclear metal.[15] Particularly, the high coordination capability of lanthanides (Ln) enables the creation of MOFs with versatile topologies.[16] Ln-MOFs have been tested for adsorbing methanol,[17] sensing xylene isomers,[18] and preferentially recognizing *p*X.[19]

To achieve selective adsorption of *m*X, we aim to design Ln-MOFs with triangular pores termed adsorbaphores,[20] in analogy to pharmacophores in drug design, which favorably interact with *m*X. Interestingly, the methyl groups of *m*X can wedge at the vertices of triangular pores and hence *m*X is more favorably adsorbed over *p*X and *o*X. It is noteworthy that a MOF, namely $Fe_2(BDP)_3$, with triangular pores was reported to selectively adsorb linear hexane against its branched isomers.[21] However, the existence of triangular pores was revealed to be not a prerequisite for the selective adsorption of hexane isomers.[22] In contrast, we envision that the triangular pores (*i.e.*, triangular adsorbaphores) in Ln-MOFs would favor

Department of Chemical and Biomolecular Engineering, National University of Singapore, 117576, Singapore. E-mail: chejj@nus.edu.sg

the selective adsorption of *m*X, as they match well with the shape of *m*X. As such, in the present study, a large number of Ln-MOFs with tunable pore size are designed for the selective adsorption of *m*X.

Results and discussion

Experimentally, a handful of Ln-MOFs (Fig. 1a) were synthesized from four different Ln metals (Dy, Er, Gd, and Ho) and H_2pzdc ligand (pyrazine-2,3-dicarboxylic acid) in the presence of Cu ions.[23,24] The resulting MOFs comprise hexanuclear Ln metal nodes and a Cu-centered Hhpzc (3-hydroxy-pyrazine-2-carboxylic acid) linker (Fig. 1b). The rigid Hhpzc linker enforces the central Cu atom to adopt an octahedral geometry, with two water molecules occupying open metal sites, and the removal of water molecules leads to a nearly square planar geometry. These Ln-MOFs possess one-dimensional (1D) triangular pores with a diameter of ~5 Å.

To validate the shape-matching concept, we computationally designed a large number of Ln-MOFs with different metal combinations (Fig. 1c). All 15 Ln elements were used for constructing the metal nodes; meanwhile, 10 different metals (Cu, Pt, Pd, Rh, Ru, Mg, Fe, Mn, Zn and Co) were considered, respectively, as the central metal (CM) atom in the linker. Among the 10 CMs, the Cu-centered linker already existed in the four experimentally reported Ln-MOFs with different metal nodes (Dy, Er, Gd, and Ho).[23,24] Altogether, 146 hypothetical structures were constructed. By adding the four experimentally synthesized MOFs, we had a total of 150 Ln-MOFs. It is worth noting that the synthesizability and stability of the hypothetical Ln-MOFs were not considered in this study. The constructed structures were geometrically optimized with the non-bonded Lennard-Jones (LJ) interactions described by the universal force field (UFF)[25] and the bond stretching mimicked by a revised harmonic potential. Details are provided in Computational methods, Fig. S1 and Table S1 (see the SI). This strategy was adopted because optimization at the electronic structure level, *e.g.*, using density functional theory (DFT), is typically challenging for Ln compounds due to their complex electronic structures.[26,27] In addition, performing DFT calculations on 150 structures would be computationally

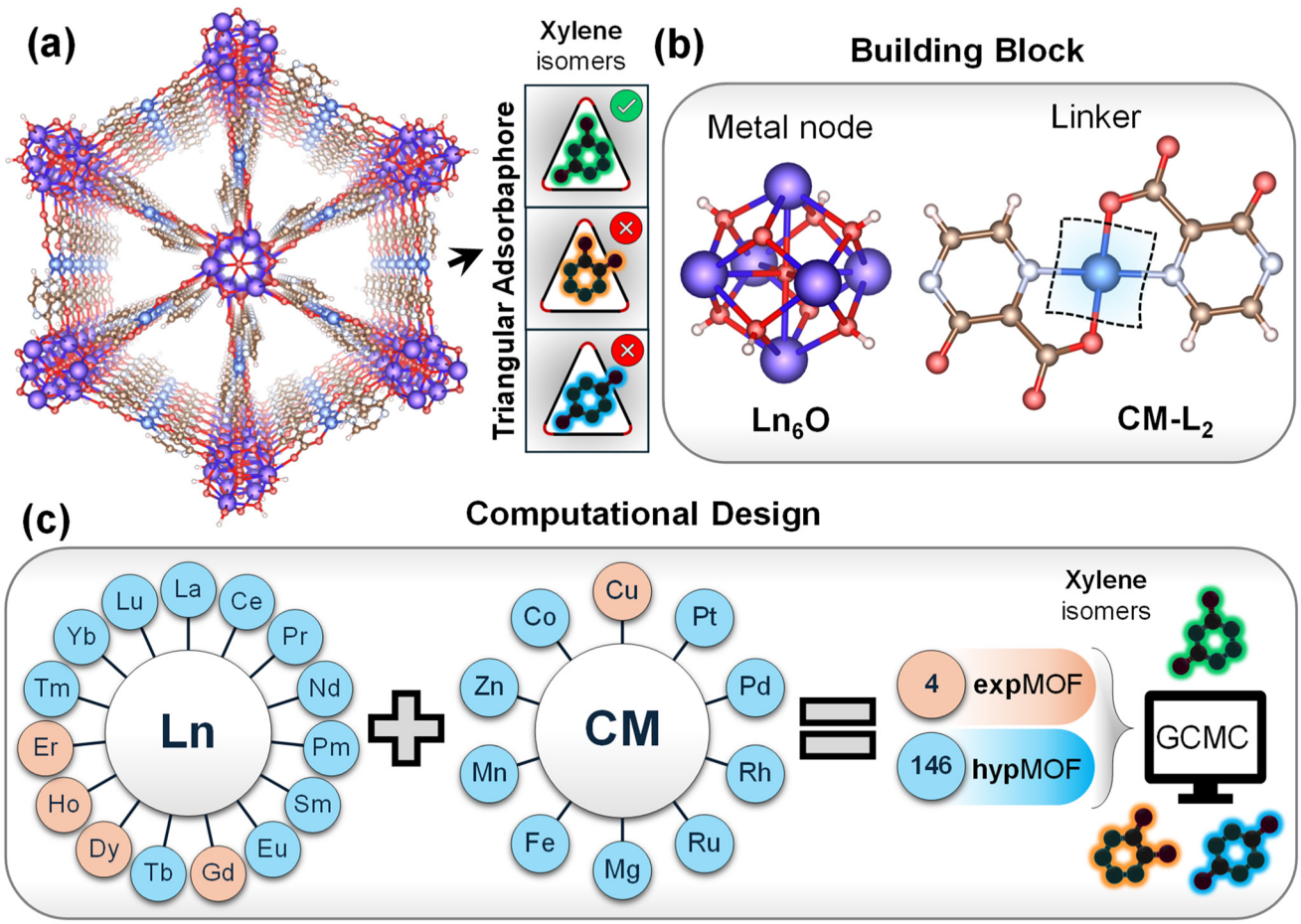

Fig. 1 (a) Ln-MOFs with triangular adsorbaphores that allow *m*X to wedge at the vertices. (b) Building blocks in a Ln-MOF consisting of a Ln metal node and a linker with a central metal (CM). (c) Design of 150 MOFs from different Ln–CM combinations, including four experimentally reported structures. Adsorption capacities of xylene isomers in these MOFs were predicted using grand canonical Monte Carlo (GCMC) simulations.

demanding. As presented in Table S2 and Fig. S2, the lattice parameters and bond lengths of our optimized structures are in excellent agreement with the reported experimental values for the four synthesized Ln-MOFs. Then, the optimized structures were used for evaluating their geometric properties (*e.g.*, pore limiting diameter, PLD). Finally, the heats of adsorption for xylene isomers at infinite dilution were calculated using the Widom insertion method. The adsorption capacities of single- and multi-component xylene isomers were predicted using grand canonical Monte Carlo (GCMC) simulations (see the SI).

Fig. 2a shows the heats of adsorption (Q_{st}°) for xylene isomers in 150 Ln-MOFs at 298 K. The highest Q_{st}°, with a mean of 85 kJ mol^{-1}, is observed for *m*X, followed by *p*X and *o*X with mean values of 76 and 72 kJ mol^{-1}, respectively. This implies that *m*X has the strongest affinity in most Ln-MOFs, as

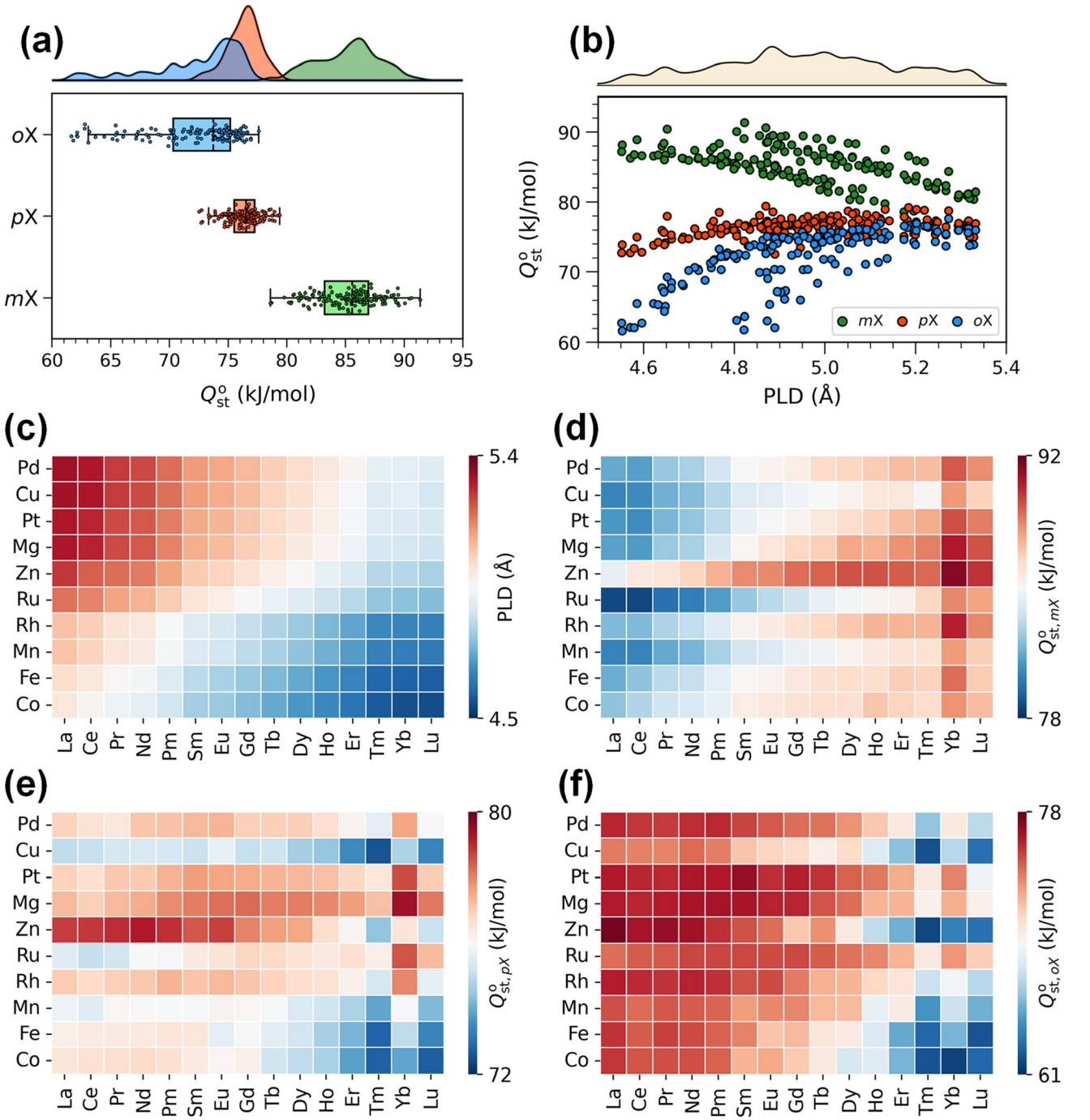

Fig. 2 (a) Q_{st}° of xylene isomers in Ln-MOFs. (b) Correlation between Q_{st}° and PLD. (c) PLD variation with metal type. (d–f) Q_{st}° variation with metal type for *m*X, *p*X and *o*X, respectively. In (c–f), Ln metals are ranked in the descending order of their ionic radii.

it can wedge at the vertices of triangular pores. The kinetic diameters d_k are 7.1, 7.4 and 6.7 Å for *m*X, *o*X and *p*X, respectively. Apparently, there are obvious variations in Q_{st}°, especially for the relatively bulkier *m*X and *o*X. To elucidate this, the PLDs of 150 Ln-MOFs were correlated with Q_{st}°. As shown at the top of Fig. 2b, the PLDs range from 4.5 to 5.4 Å, with most populated around 5 Å. We should note that d_k is a rough measure of molecular size; even if PLDs are smaller than the d_k of an isomer, many MOFs can still accommodate the isomer. From Fig. 2b, the three isomers exhibit a larger difference in Q_{st}° at a smaller PLD, but the difference reduces with increasing PLD. For *m*X, a higher Q_{st}° is seen in a narrower pore, which allows *m*X molecules to tightly wedge at the pore vertices; however, this tight packing becomes loose when the pore size increases. For *o*X, Q_{st}° increases with PLD, as a wider pore can accommodate bulkier *o*X molecules. Different from *m*X and *o*X, *p*X shows only weak variation of Q_{st}° with PLD, due to its smallest molecular size among the three isomers.

Apparently, pore size is crucial in governing the adsorption selectivity of xylene isomers. A narrower pore tends to display higher selectivity, and $S_{mX/oX}$ is anticipated to be greater than $S_{mX/pX}$. Conversely, a wider pore reduces the interaction difference between xylene isomers and is not suitable for separation. To boost xylene selectivity, the pore size can be adjusted. As demonstrated experimentally, the pore size in MFM-300 was tuned upon altering metal type, thus leading to a significant change of xylene selectivity.[28] It is instructive to examine how the pore size is affected by the metal type in this study. Fig. 2c shows the PLD variation with metal type for 150 Ln-MOFs. MOFs with La and Ce have the largest PLDs, while those with Yb and Lu have the smallest. Notably, PLD is found to positively correlate with the ionic radius of the Ln metal (Fig. S3a). With descending ionic radius, PLD decreases. This is because a smaller radius of Ln metal induces a shorter coordination bond, a contracted lattice, and a narrower pore. In contrast, there is no apparent correlation between the PLD and the radius of CM (Fig. S3b). The largest PLD is associated with Pd, Cu and Pt, followed by Mg, Zn and Ru, while the smallest PLD is for Rh, Mn, Fe and Co. In 150 Ln-MOFs with different Ln–CM combinations, La and Ce with Pd, Cu, Pt and Mg possess wider pores, while Lu and Yb with Co have narrower ones (Fig. S3c).

Additionally, we analyze the Q_{st}° of xylene isomers based on metal combinations. As shown in Fig. 2d for *m*X, among Ln metals, MOFs with Yb exhibit the highest Q_{st}°, followed by Lu. This is because these metals form narrower pores in which *m*X molecules can wedge at the vertices. Among CMs, Zn possesses the strongest affinity for *m*X; thus, the MOF with Yb–Zn shows the highest Q_{st}°. Interestingly, although MOFs with Lu–Co and Yb–Co have the smallest PLDs, the highest Q_{st}° is observed in the MOF with Yb–Zn. The reason is that the interaction of *m*X with Zn is stronger than with Co, as reflected by the LJ potential parameters (ε) of ~0.52 and ~0.06 kJ mol^{-1}, respectively. This observation reveals the important role of metal chemistry, besides pore geometry, in governing adsorption performance. For *p*X, Q_{st}° in Fig. 2e shows a relatively small range of variation (~8 kJ mol^{-1}) compared to that for *m*X. Similarly, many of the MOFs with Yb exhibit stronger interaction with *p*X, particularly those with Yb–Mg. Across the CMs, on average, Zn has the strongest affinity, as explained earlier. For *o*X, as shown in Fig. 2f, the opposite trend of Q_{st}° is observed. Specifically, a Ln metal forming a wider pore favors *o*X adsorption than its counterpart forming a narrow pore. This is because *o*X is relatively bulkier and encounters repulsion in a narrower pore, whereas a pore with adequate size (5.2–5.4 Å) maximizes interaction with *o*X. On one hand, La adjusts the pore to a suitable size for *o*X adsorption; on the other hand, Zn has the strongest interaction with xylene; consequently, the combination of La–Zn exhibits the highest affinity for *o*X and hence the highest Q_{st}°. Overall, by examining Q_{st}° for the three xylene isomers, we can identify which combination of metals allows the selective adsorption of *m*X over *p*X and *o*X. For instance, the combination of an Ln metal (such as Lu, Yb, Tm or Er) forming a narrower pore with a CM possessing strong interaction with *m*X (such as Zn) is effective in discriminating xylene isomers.

Fig. 3a presents the adsorption capacities of single-component (*i.e.*, pure) xylene isomers at 298 K and 1 bar. Along the *x*-axis, Ln metals are ranked in the descending order of their ionic radii, and for each Ln metal, there are 10 MOFs with different CMs in the linker. A significant variation in the adsorption capacity of each isomer is observed, signifying the combined effects of both Ln and CM on pore geometry and interaction strength. The capacity decreases with descending ionic radius of Ln metal, originating from the positive correlation between PLD and ionic radius (Fig. S3a), as a wider pore accommodates more molecules. Because of its smallest molecular size, *p*X exhibits the greatest capacity than *m*X and *o*X (Fig. S4a). The difference in capacity between *p*X and bulkier isomers is especially notable in MOFs with a Ln metal of a larger ionic radius (*e.g.*, La metal) and hence a wider pore. However, this difference diminishes as the pore becomes narrower (*e.g.*, Lu metal). The two bulkier isomers *m*X and *o*X display almost identical capacity in MOFs with medium to wide pores. In MOFs with a narrow pore, *o*X exhibits the lowest capacity. In all cases, the capacity ranges from 0.5 to 1.25 mol kg^{-1}, which is greater than the typical threshold (0.5–0.6 mol kg^{-1})[12,14] commonly used to identify top-performing MOFs for xylene separation.

The conformations of xylene molecules adsorbed in a representative Ln-MOF (Dy–Cu) are illustrated in Fig. 3b. Shape matching is obviously observed for *m*X, with its methyl groups wedged at the vertices. However, *m*X molecule adopts an inclined orientation, does not completely face the pore opening, and positions its two methyl groups toward non-opposing Ln metals on either side of the pore (Fig. 3c). This orientation might occur due to the presence of a CM in the linker, which interacts strongly with *m*X. In contrast, *p*X and *o*X tend to lie along the pore direction, because their methyl groups do not match the triangular shape. These observations corroborate the higher Q_{st}° of *m*X compared to those of *p*X and *o*X. Nevertheless, xylene separation cannot be determined simply based on the adsorption of pure isomers. As presented

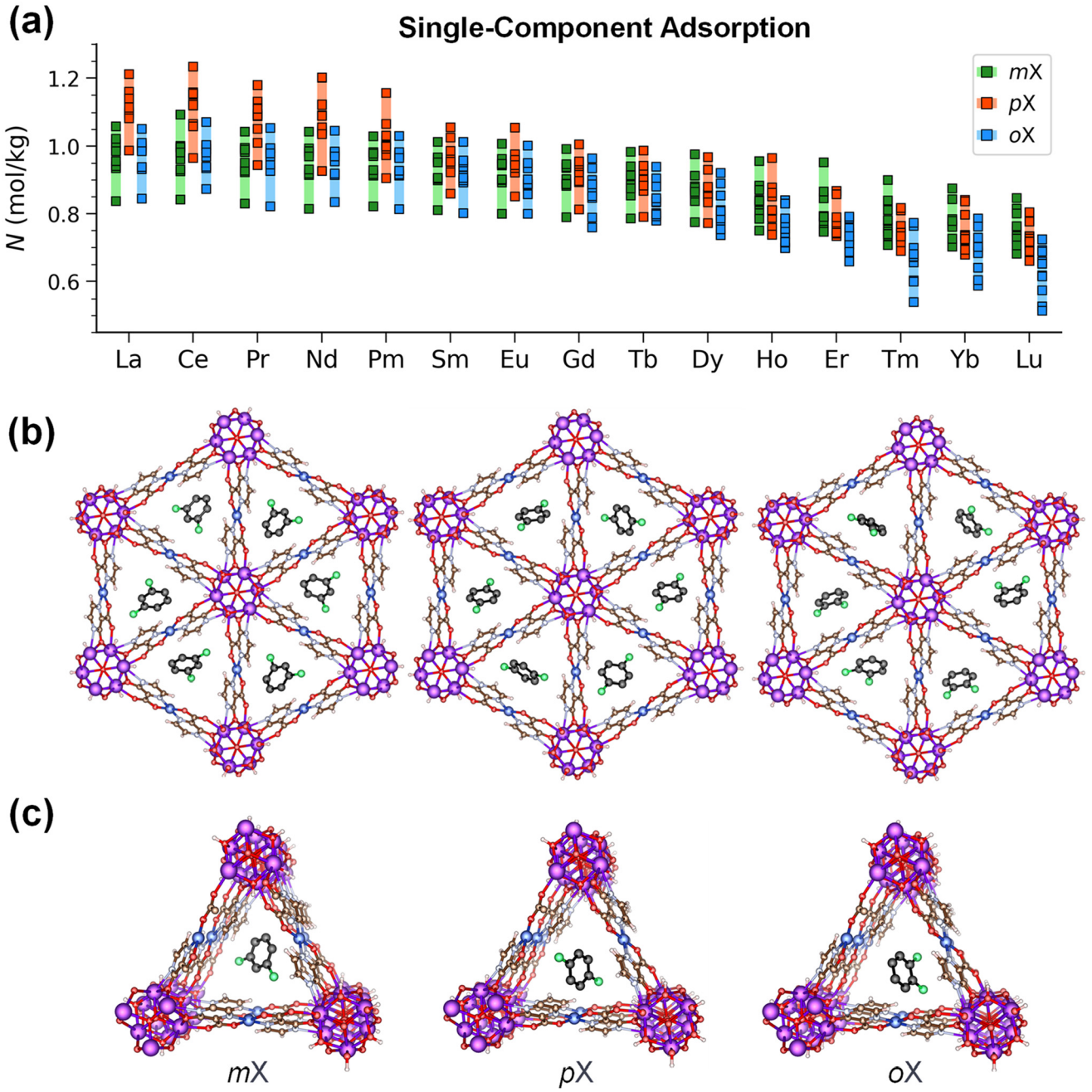

Fig. 3 Adsorption of singe-component xylene isomers at 298 K and 1 bar. (a) Adsorption capacities in MOFs grouped by their Ln metal type. (b) Conformations of xylene molecules adsorbed in a representative MOF with Dy–Cu metals. (c) Orientations of xylene molecules in triangular pores.

below, the competitive adsorption among isomers in a mixture is remarkable and must be taken into account.

Fig. 4a presents the adsorption capacities of multi-component xylene isomers (*i.e.*, an equimolar mixture) at 298 K and 1 bar. For MOFs comprising La and Ce (*i.e.*, Ln metals with the largest radii), *p*X exhibits the highest capacity. This is because the pores formed by La and Ce are unsuitable for compact packing of *m*X, thereby losing the merit of triangular adsorbaphores. In such cases, the MOFs are *p*X selective. When the ionic radius of Ln metal descends, *p*X capacity decreases, while *m*X capacity increases. The highest distinction is observed in MOFs with Yb and Lu, where *m*X can fit tightly in their pores. Notably, the capacities of both *p*X and *m*X vary among 10 different CMs in the linker, due to different interaction strengths of CMs. Nevertheless, the variation is marginal in La-MOFs and Ce-MOFs, due to a small interaction strength difference in these MOFs with wide pores. For MOFs with Pr–Tb metals, the variation is significant, as the pore size is intermediate and the energetic factor dominates adsorption. In contrast, in MOFs with narrow pores, the geometric factor

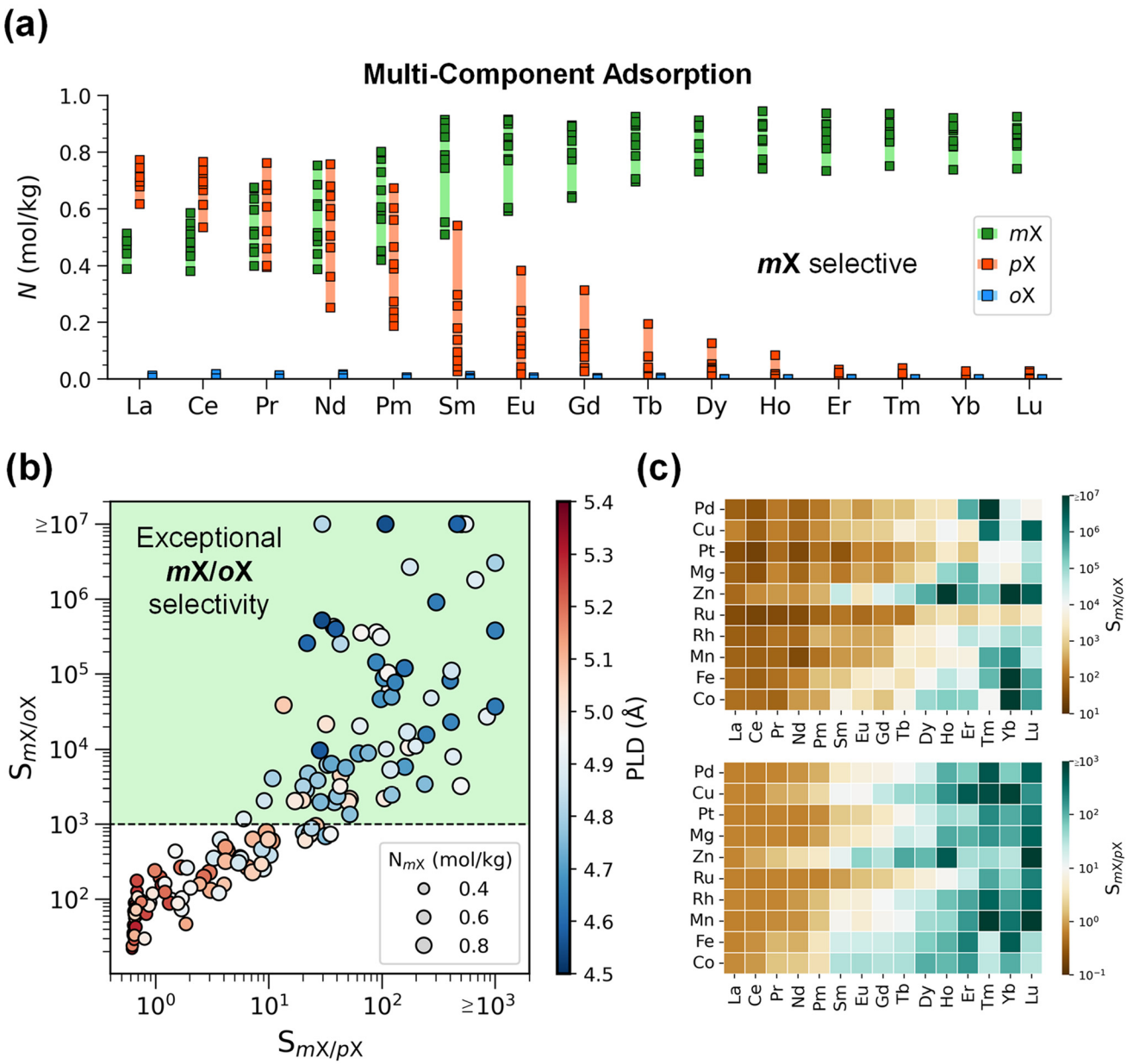

Fig. 4 Adsorption of multi-component xylene isomers (equimolar mixture) at 298 K and 1 bar. (a) Adsorption capacities in MOFs grouped by the Ln metal type. (b) $S_{mX/oX}$ *versus* $S_{mX/pX}$. (c) $S_{mX/oX}$ and $S_{mX/pX}$ variation with metal type. Ln metals are ranked in the descending order of their ionic radii.

(*i.e.*, pore size) plays a vital role in selective adsorption of *m*X, while metal interaction plays a minor role, minimizing the variation in capacity across different CMs in the linker. It is interesting to observe that *o*X adsorption is negligible in all the Ln-MOFs with different combinations of metals. This is a result of strong competitive adsorption among the three isomers. With shape matching, *m*X is the most favorably adsorbed isomer (except in MOFs with La and Ce Ln metals); thus, *m*X replaces *p*X, particularly in a narrow pore. With the bulkiest molecular size, *o*X is the least adsorbed isomer. Therefore, the competition can be attributed to both energetic and entropic effects. Overall, *m*X has the highest capacity in 150 Ln-MOFs, followed by *p*X, and the capacity of *o*X is vanishingly low (Fig. S4b).

Fig. 4b presents the selectivity of *m*X/*o*X ($S_{mX/oX}$) plotted against the selectivity of *m*X/*p*X ($S_{mX/pX}$) in all the Ln-MOFs. All the MOFs possess $S_{mX/oX} > 10$, with many showing exceptionally high $S_{mX/oX}$ values exceeding 1000. The majority of the MOFs also show significant $S_{mX/pX}$, but reverse selectivity is found in MOFs with large pores. It is revealed that the selectivity is largely governed by pore size but also depends on guest–host interaction. Additionally, all the MOFs are *p*X selective toward o*X*. Fig. 4c illustrates $S_{mX/oX}$ and $S_{mX/pX}$ variation with metal type, where Ln metals of small radii leads to high selectivity.

Conclusion

We have computationally designed a series of Ln-MOFs featuring one-dimensional triangular adsorbaphores. By tuning the metal types in both metal node and linker, the pore size can be adjusted to selectively adsorb *m*X. From simulations, the affinities of Ln-MOFs for xylene isomers and their adsorption capacities are evaluated. It is confirmed that *m*X has the strongest interaction among the three isomers with these MOFs. The adsorption of multi-component xylene isomers demonstrates significantly high *m*X/*o*X and *m*X/*p*X selectivities. The MOFs also exhibit promising *p*X/*o*X separation capability. As such, three xylene isomers can be separated completely using a two-step adsorption process, the first step separates *m*X from *p*X and *o*X, and the second one separates *p*X and *o*X. Importantly, the selectivities among xylene isomers in these Ln-MOFs can be effectively controlled using different metal combinations. While the present work is entirely computationally driven, we wish that it would trigger experimental investigation. We acknowledge that the synthesis of these Ln-MOFs, especially the hypothetical ones, may pose a challenge due to the complex nature of frameworks and the limited availability of Ln metal precursors, which are less sustainable for mass production. Nevertheless, the design strategy might open a new direction for the efficient separation of xylene isomers and other important mixtures in the chemical industry.

Author contributions

SAM: conceptualization, methodology, investigation, formal analysis, visualization, and writing – original draft. JJ: funding acquisition and writing – review and editing.

Conflicts of interest

The authors declare no competing financial interest.

Data availability

The data supporting this article have been included in the manuscript and the SI. Supplementary Information file contains computational methods, geometric properties, and statistics of adsorption capacities. See DOI: **https://doi.org/10.1039/d5nr02310f**.

Acknowledgements

We gratefully acknowledge the National Research Foundation Singapore (NRF-CRP26-2021RS-0002) for financial support and the National University of Singapore and the National Supercomputing Centre (NSCC) Singapore for computational resources.

References

1 Q. Shi, J. C. Gonçalves, A. F. P. Ferreira and A. E. Rodrigues, *Chem. Eng. Process.*, 2021, **169**, 108603.
2 J. Johnson and P. Whitchurch, *Industrial Arene Chemistry*, Wiley, 2023, vol. 11, pp. 453–478.
3 Y. Yang, P. Bai and X. Guo, *Ind. Eng. Chem. Res.*, 2017, **56**, 14725–14753.
4 A. Nalaparaju and J. Jiang, *Adv. Sci.*, 2021, **8**, 2003143.
5 Z. Zhang, S. B. Peh, C. Kang, K. Chai and D. Zhao, *EnergyChem*, 2021, **3**, 100057.
6 X. Yang, H.-L. Zhou, C.-T. He, Z.-W. Mo, J.-W. Ye, X.-M. Chen and J.-P. Zhang, *Research*, 2019, **2019**, 9463719.
7 R. Lyndon, Y. Wang, I. M. Walton, Y. Ma, Y. Liu, Z. Yu, G. Zhu, S. Berens, Y. S. Chen, S. Y. G. Wang, S. Vasenkov, D. S. Sholl, K. S. Walton, S. H. Pang and R. P. Lively, *Chem. Commun.*, 2022, **58**, 12305–12308.
8 K. B. Idrees, Z. Li, H. Xie, K. O. Kirlikovali, M. Kazem-Rostami, X. Wang, X. Wang, T.-Y. Tai, T. Islamoglu, J. F. Stoddart, R. Q. Snurr and O. K. Farha, *J. Am. Chem. Soc.*, 2022, **144**, 12212–12218.
9 L. Yu, J. Zhang, S. Ullah, J. Yao, H. Luo, J. Huang, Q. Xia, T. Thonhauser, J. Li and H. Wang, *Angew. Chem., Int. Ed.*, 2023, **62**, e202310672.
10 H. Jin, S. Kim, Y. Choi, K. Kim and Y. Bae, *J. Ind. Eng. Chem.*, 2023, **117**, 333–341.
11 J. A. Gee, K. Zhang, S. Bhattacharyya, J. Bentley, M. Rungta, J. S. Abichandani, D. S. Sholl and S. Nair, *J. Phys. Chem. C*, 2016, **120**, 12075–12082.
12 Z. Qiao, Y. Yan, Y. Tang, H. Liang and J. Jiang, *J. Phys. Chem. C*, 2021, **125**, 7839–7848.
13 P. Halder and J. K. Singh, *Energy Fuels*, 2023, **37**, 2230–2236.
14 S. A. Mohamed, R. Zheng, N. Zhu, D. Zhao and J. Jiang, *J. Am. Chem. Soc.*, 2025, **147**, 12251–12262.
15 F. Saraci, V. Quezada-Novoa, P. R. Donnarumma and A. J. Howarth, *Chem. Soc. Rev.*, 2020, **49**, 7949–7977.
16 K. Patra and H. Pal, *RSC Sustainability*, 2025, **3**, 629–660.
17 C. G. Efthymiou, E. J. Kyprianidou, C. J. Milios, M. J. Manos and A. J. Tasiopoulos, *J. Mater. Chem. A*, 2013, **1**, 5061–5069.
18 J. Zhang, J. Wang, S. Long, S. B. Peh, J. Dong, Y. Wang, A. Karmakar, Y. Di Yuan, Y. Cheng and D. Zhao, *Inorg. Chem.*, 2018, **57**, 13631–13639.
19 M. Wang, Z. Han, K. Wang, B. Zhao, T. Sun, Y. Wu, P. Cheng and W. Shi, *Angew. Chem., Int. Ed.*, 2024, **63**, e202318722.
20 P. G. Boyd, A. Chidambaram, E. García-Díez, C. P. Ireland, T. D. Daff, R. Bounds, A. Gładysiak, P. Schouwink, S. M. Moosavi, M. M. Maroto-Valer, J. A. Reimer, J. A. R. Navarro, T. K. Woo, S. Garcia, K. C. Stylianou and B. Smit, *Nature*, 2019, **576**, 253–256.
21 Z. R. Herm, B. M. Wiers, J. A. Mason, J. M. van Baten, M. R. Hudson, P. Zajdel, C. M. Brown, N. Masciocchi, R. Krishna and J. R. Long, *Science*, 2013, **340**, 960–964.

22 Y. G. Chung, P. Bai, M. Haranczyk, K. T. Leperi, P. Li, H. Zhang, T. C. Wang, T. Duerinck, F. You, J. T. Hupp, O. K. Farha, J. I. Siepmann and R. Q. Snurr, *Chem. Mater.*, 2017, **29**, 6315–6328.
23 L. F. Chen, J. Zhang, G. Q. Ren, Z. J. Li, Y. Y. Qin, P. X. Yin, J. K. Cheng and Y. G. Yao, *CrystEngComm*, 2008, **10**, 1088–1092.
24 Y. Bing, N. Xu, W. Shi, K. Liu and P. Cheng, *Chem. – Asian J.*, 2013, **8**, 1412–1418.
25 A. K. Rappé, C. J. Casewit, K. S. Colwell, W. A. Goddard and W. M. Skiff, *J. Am. Chem. Soc.*, 1992, **114**, 10024–10035.
26 M. Ferbinteanu, A. Stroppa, M. Scarrozza, I. Humelnicu, D. Maftei, B. Frecus and F. Cimpoesu, *Inorg. Chem.*, 2017, **56**, 9474–9485.
27 A. Rajabi, R. Grotjahn, D. Rappoport and F. Furche, *Dalton Trans.*, 2023, **53**, 410–417.
28 X. Li, J. Wang, N. Bai, X. Zhang, X. Han, I. da Silva, C. G. Morris, S. Xu, D. M. Wilary, Y. Sun, Y. Cheng, C. A. Murray, C. C. Tang, M. D. Frogley, G. Cinque, T. Lowe, H. Zhang, A. J. Ramirez-Cuesta, K. M. Thomas, L. W. Bolton, S. Yang and M. Schröder, *Nat. Commun.*, 2020, **11**, 1–10.